Research Article | Vol. 30, No. 19 / 12 Sep 2022 / Optics Express 33708
Optics EXPRESS

Highly coherent, flat, and broadband time-stretched swept source based on extra-cavity spectral shaping assisted by a booster semiconductor optical amplifier

HONGJIE CHEN,[1,2] YUJIA LI,[1,2] DONGMEI HUANG,[1,2,*] YIHUAN SHI,[1,2] FENG LI,[2,3] CHAO LU,[2,3] AND P. K. A. WAI[2,3,4]

[1]*Photonics Research Institute, Department of Electrical Engineering, The Hong Kong Polytechnic University, Hong Kong SAR, China*
[2]*The Hong Kong Polytechnic University Shenzhen Research Institute, Shenzhen 518057, China*
[3]*Photonics Research Institute, Department of Electronic and Information Engineering, The Hong Kong Polytechnic University, Hong Kong SAR, China*
[4]*Department of Physics, Hong Kong Baptist University, Hong Kong SAR, China*
[*]*meihk.huang@polyu.edu.hk*

Abstract: We demonstrate a flat broadband time-stretched swept source based on extra-cavity spectral shaping. By adjusting the polarization-dependent gain profile and driving current of the booster optical amplifier (BOA), extra-cavity spectral shaping is optimized to generate output with a 1-dB bandwidth of ~100 nm, 3-dB bandwidth of ~140 nm and output power of ~21.4 mW. The short-term and long-term stabilities are characterized. The average cross correlation of 183,485 round trips is 0.9997 with a standard deviation of 2×10^{-5}, indicating high single-shot spectral similarity and high coherence. The noise floor of relative spectral energy jitter is −141.7 dB/Hz, indicating a high short-term spectral energy stability. The proposed highly stable flat broadband time-stretched swept source is applied to an optical coherence tomography (OCT) system. The axial resolution is 10.8 μm. The proposed swept source can serve as excellent light sources in ultra-fast coherent detection systems for high precision sensing and imaging.

1. Introduction

Broadband coherent light sources have been widely investigated and applied in many fields, such as biomedical imaging, spectroscopy, and metrology [1–13]. Broadband time-stretched swept source is a preferred light source for optical sensing including multiple fiber Bragg gratings (FBGs) interrogation systems and most important high resolution swept source OCT (SS-OCT) systems. Conventional broadband swept sources based on tunable filters including short cavity and Fourier domain mode locked lasers have been proposed. The main bottleneck is the sweep rate which is limited to tens of kilohertz because of the mechanical tuning mechanism [7,14–16]. Swept sources based on micro-electro-mechanical system (MEMS) filters or vertical-cavity surface-emitting lasers (VCSEL) can achieve sweep rate at hundreds of kilohertz, but sweep rate at megahertz remains challenging [14,16–18]. A promising method to generate megahertz or even hundreds of megahertz swept sources is to utilize the time stretching technique, in which different spectral components of the short pulse are spread to different temporal positions by dispersion to form a swept signal [19,20]. The coherence of the spectral components of the ultrashort pulse determines not only the stability of the swept signal but also the imaging range of the OCT systems. To obtain a high axial resolution OCT image, the spectral bandwidth of the seed laser should be sufficiently large. The engineering of such a swept source mainly focuses on the improvement of spectral bandwidth and coherence of the broadband pulse.

#468042 https://doi.org/10.1364/OE.468042
Journal © 2022 Received 15 Jun 2022; revised 6 Aug 2022; accepted 8 Aug 2022; published 29 Aug 2022

Optics EXPRESS

A short coherent pulse can be obtained in a mode-locked laser cavity. However, the gain bandwidth of rare-earth-doped fibers is normally in the order of tens of nanometers only, which makes the realization of >100 nm mode-locked laser output challenging. Spectral broadening by utilizing the nonlinearity and dispersion management inside the laser cavity is commonly used to enhance the mode-locked pulse bandwidth. By precisely controlling the dispersion and nonlinearity in the cavity, many broadband mode-locked fiber lasers have been proposed and demonstrated [2,4,6,21–31]. The 3-dB bandwidth of the spectrum can reach tens of nanometer to even over 100 nm [21,26,29] but with strong modulations on the spectrum. Additionally, cavities with optical free-space elements are susceptible to environmental disturbance. Mamyshev oscillator is another effective method to generate broadband pulse spectrum [32–36]. However, the structure of the Mamyshev oscillator is complex and the oscillator does not self-start easily owing to the spectral filtering. Another challenge faced by the Mamyshev oscillator is the difficulty to realize a highly coherent flat spectrum. An extra-cavity gain-managed nonlinear fiber amplifier has been used to obtain a broadband spectrum with a 3-dB bandwidth of more than 100 nm [11,37,38]. Inside the gain-managed nonlinear fiber amplifier, the nonlinear spectral broadening is determined by the pulse energy, dispersion, and nonlinearity, making it difficult to simultaneously optimize all the parameters. Semiconductor optical amplifier (SOA) can be used as an extra-cavity spectral shaping tool to broaden and flatten the spectrum. In 2018, Kang, J. demonstrated a broadband, flat, time-stretched swept source by using an SOA outside the laser cavity, the 3-dB bandwidth of the swept source can reach up to 100 nm [2]. However, the spectrum has a large slope and poor spectral flatness. Thus, it remains challenging to obtain broadband swept source with a 1-dB bandwidth of tens of or even a hundred nanometers.

In this paper, we demonstrate a high-performance time-stretched swept source with a flat broadband spectrum, high short-term and long-term stability, and high coherence with extra-cavity spectral shaping by optimizing the polarization and driving current of the booster SOA. This high performance swept source is then applied to OCT imaging and achieves 183.6 MHz imaging speed and 10.8 μm axial resolution, which will find applications in ultrafast imaging systems. The rest of the paper is organized as follows. Section II describes the experimental setup. The output performance of the time-stretched swept source including the optical spectrum, RF spectrum, short-term and long-term stability and the SS-OCT characterizations are demonstrated in Section III. Section IV concludes the paper.

2. Experimental setup

Figure 1(a) shows the schematic diagram of the time-stretch broadband swept source, which comprises a broadband mode locked laser, a 1.49 km long single mode fiber (SMF) to stretch the picosecond pulse to a long chirped pulse and obtain wavelength sweeping, a booster semiconductor amplifier (BOA) to amplify the sweep signal. A nonlinear polarization rotation mode-locked laser is used as the seed laser to generate a flat and broadband swept source by using extra-cavity spectrum shaping. The parameters of the mode-locked laser can be found in our recent work [4]. Note that 20% of the light is reflected by the tap-isolator wavelength division multiplexer (TIWDM) for measurement purpose. The seed laser is launched into a SMF first instead of directly to the booster semiconductor amplifier (BOA) because of the following reasons. First, the SMF is used to stretch the short pulse and reduce the peak power to avoid nonlinear spectrum expansion by self-phase modulation and other nonlinear effects, which may deteriorate the coherence of the laser. Second, lowering the power of the seed laser can protect the BOA from damage. Third, after the time stretching with the SMF, a BOA can compensate for the loss and achieve high output power, which will improve the sensitivity of the SS-OCT system. A C-band BOA (BOA1004S, Thorlabs) centered at 1550 nm with a polarization-dependent gain is utilized to reshape the swept signal outside the cavity. By varying the polarization of the light injected into the BOA with the polarization controller (PC), the gain profile can be adjusted according to the time-stretched swept

Optics EXPRESS

signal to generate a flat broadband spectrum. The output spectra and temporal time-stretched pulse are detected by an optical spectrum analyzer (ANDO, AQ-6315B, Optical Spectrum Analyzer) and a real-time oscilloscope (OSC,106 Keysight, DPO759SA-X 96204Q), respectively. For the time-average measurement of pulse spectrum, the spectra from output A (directly from the seed fiber laser) and output B (after the BOA) are measured by an OSA, while for the real-time spectrum measurement, the temporal time-stretch signal before and after BOA are captured by an OSC with a bandwidth of 62 GHz and sample rate of 160 GS/s. The measurement before and after the BOA are carried out separately. The measurement before the BOA is carried the two dashed lines and the SMF only. The measurement after the BOA is done with the connection indicated by the solid lines.

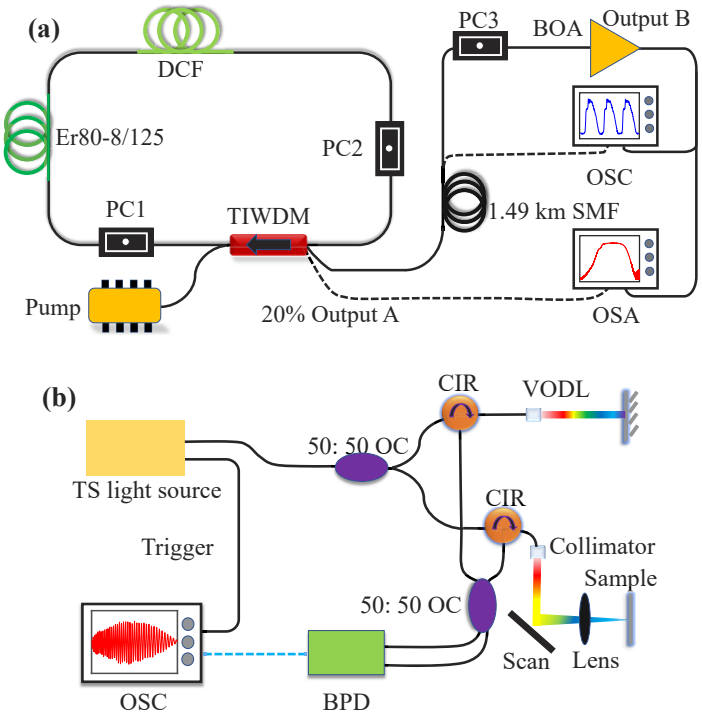

Fig. 1. Schematic diagram of the broadband swept source and OCT system. (a) The time-stretched light source and the measurement system, DCF: Dispersion compensation fiber, PC: Polarization controller, TIWDM: Tap-isolator wavelength division multiplexer, SMF: Single mode fiber, BOA: Booster optical amplifier, OSA: Optical spectrum analyzer, OSC: Oscilloscope. (b) SS-OCT system, OC: Optical coupler, CIR: Circulator, VODL: Variable optical delay line, BPD: Balanced photodetector.

Figure 1(b) shows the schematic diagram of the SS-OCT system. The system includes a broadband swept source as shown in Fig. 1(a), a Michelson interferometer with a scanning galvo mirror, and a high-speed acquisition system with a balanced photodetector (BPD) and real-time oscilloscope. 1% of the seed fiber laser output is used to synchronically trigger the real-time oscilloscope to capture the interference signals acquired by the BPD, while 99% of the seed fiber laser output is launched into the 1.49 km SMF and then is injected into the BOA. A 50:50 optical coupler is used to divide the amplified broadband swept signal into two arms. One is the reference arm including an optical circular and an optical mirror, while the other is the sample arm including an optical circular, a collimator (Thorlabs, F280APC-C), the scanning mirror

Optics EXPRESS

(Thorlabs, GVS102), and the sample. The interference signal is detected by a BPD (Finisar, BPDV2150R) with 43 GHz bandwidth and acquired by a real-time oscilloscope.

3. Experimental results and discussions

3.1. Optical spectrum, RF spectrum and the stretched pulses

To achieve a broadband swept laser based on extra-cavity amplification, the output of the seed laser should have a broadband spectrum, which can be generated by optimizing the dispersion and nonlinearity of the seed laser. The dispersion management is obtained by inserting a section of dispersion compensating fiber (DCF) in the cavity to ensure that the net dispersion is near zero. By increasing the pump power to 1.28 W and precisely adjusting the polarization state to control the nonlinearity. Figure 2(a) shows that a broadband mode-locked laser is obtained with a 3-dB bandwidth of 107.2 nm (blue curve on linear scale) and 1-dB bandwidth of 8.1 nm (red curve on logarithmic scale), as measured by the OSA. An electrical spectrum analyzer (ESA, Keysight, N9020B) is used to measure the radio frequency (RF) spectrum. Figure 2(b) shows that the signal-to-noise ratio (SNR) of the pulse train can be as high as ~86 dB at the fundamental repetition rate of 183.6 MHz, indicating that the seed laser is operating at the stable mode locking state. The resolution bandwidth is 10 kHz. The output power from the seed laser is about 30 mW, which is attenuated by a variable optical attenuation and then injected to the 1.49-km SMF. The optical power is at ~5 mW before the BOA. Figure 2(c) shows that the picosecond pulses are chirped to several nanoseconds long by the time stretching process owing to the large dispersion of the long SMF. It should be noted that pulse spectrum mapped into the temporal domain is captured by the real-time OSC. The envelope of the stretched pulse is similar to the spectral profile of the seed laser, which shows that the time stretching process is linear and the coherence of stretched pulse remains high.

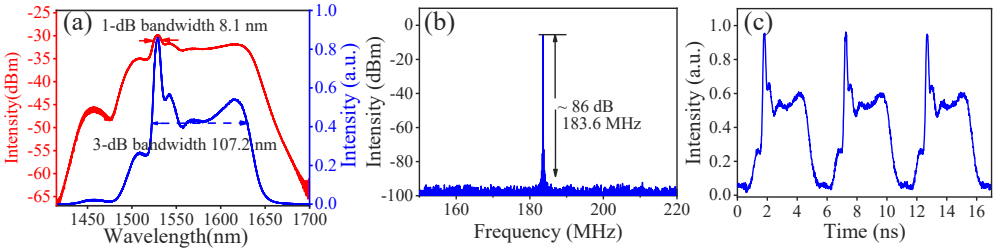

Fig. 2. (a) The direct output optical spectrum of the seed laser. (a) The spectrum in linear (blue curves) and logarithmic (blue curves). (b) The RF spectrum of the mode-locked seed laser. (c) The time stretched pulses after the SMF.

Extra-cavity amplification assisted by the BOA will generate an ultrabroad spectrum when the gain profile of the BOA is precisely controlled with an appropriate driving current and the polarization controller. As shown in Fig. 2(a), the intensity of the seed spectrum in the shorter wavelength is larger than that in the longer wavelength as clearly shown by the blue curve. The spectrum can be flattened by using a BOA. We choose a BOA with a 3-dB bandwidth of 85 nm centered at a wavelength around 1550 nm, small gain of 27 dB, and saturation output power of 15 dBm as the amplifier. The gain profile of the BOA can be adjusted by changing the driving current and the polarization state of the input light. To demonstrate the effect of the polarization state of the input light on the BOA, the amplified spectra at different input polarization states as measured by the OSA are shown in Fig. 3(a). The driving current is 500 mA. A flat and broadband spectrum can be achieved as shown in the blue curve. As the polarization controllers used in our experiment are based on optical fibers instead of waveplates, the polarization angles

Optics EXPRESS

at the four polarization states cannot be provided. Figure 3(b) shows that the profile of the spectrum recorded by the OSA can also be reshaped by varying the driving current of the BOA, where the 3-dB bandwidth increases from 52.3 to 136.7 nm when the driving current increases from 50 to 500 mA. When the driving current increases from zero, the spectrum is broadened initially. When the driving current increases beyond ~300 mA, the bandwidth and output power of the spectrum vary only slightly because the BOA is saturated. Figure 3(c) presents the output power (red curves) and SNR (blue curves) of the amplified pulses at different driving currents. The SNR increases significantly as the driving current increases from 0 to 150 mA, and then converges slowly towards a relatively steady value of ~80 dB. When the driving current is less than 150 mA, the BOA is unable to effectively amplify the signal but it also lowers the power of the input signal, which results in low SNR. Beyond 150 mA, the SNR remains at ~80 dB level even if we further increase the driving current as shown by the blue curve in Fig. 3(c). From Fig. 3(c), the output power of the amplified swept signal (red curves) increases as the driving current increases. When the driving current reaches the damage threshold of BOA at 500 mA, the output power of the amplified swept signal is 21.4 mW.

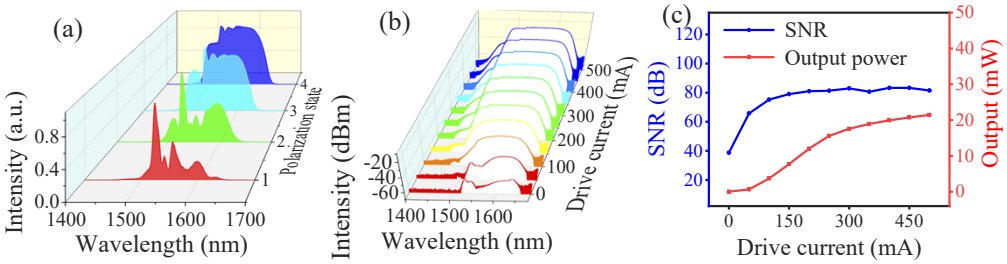

Fig. 3. Amplified spectra with the BOA. (a) Spectra at different polarization states. (b) Spectra with different driving current. (c) Output power and SNR versus driving current.

Guided by the experimental results in Fig. 3, we tune the BOA at the maximum driving current of 500 mA and adjust the polarization state of the light. The gain profile of the BOA can be adjusted according to the time stretched swept signal to generate a flat and broadband spectrum assisted by a PC. We note that the active layer of the booster optical amplifier has rectangular shape with large width but small thickness, and it consists of multiple quantum well layers of InP/InGaAsP, which increases the anisotropy [39]. Gain-saturation of the BOA also plays an important role in flattening the spectrum. Figure 4(a) shows that a flat broadband spectrum is obtained with a 1-dB bandwidth of 93.1 nm and a 3-dB bandwidth of 136.7 nm as shown by the red curves on linear scale. The blue curves in Fig. 4(a) is the seed spectrum before the BOA plotted in linear scale for comparison. To the best of our knowledge, this is the first realization of an ultra-flat broadband time-stretched swept source with 1-dB bandwidth of nearly 100 nm. Figure 4(b) shows the measured RF spectrum. The SNR remains high at 80 dB indicating that the stretched swept signal is highly coherent with only small jitters after the amplification. The result shows that the BOA can realize linear amplification without deteriorating the coherence of the seed laser, which is important for applications such as SS-OCT systems where a highly coherent broadband swept source is required to achieve high axial resolution and long imaging range. The spectral shaping by the BOA flattened the waveform of the swept signal as shown in Fig. 4(c) when compared with that in Fig. 2(c). Likewise, the real-time OSC captured the measured waveform in Fig. 4(c).

To see the polarization characteristic of the amplification swept signal after the BOA, we have measured the spectrum from the two output branches of the PBS. The experimental setup of the external polarization system is shown in Fig. 5(a). A polarization controller is inserted between the light source and the polarization beam splitter (PBS) to adjust the polarization state of the

Optics EXPRESS

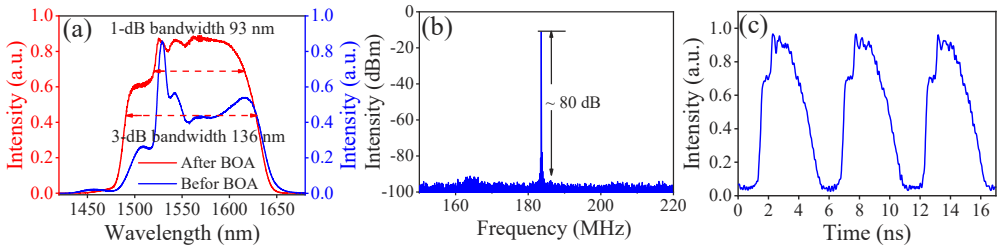

Fig. 4. Optimized time stretched swept source assisted by extra-cavity spectral shaping after the BOA. (a) The flat broadband spectrum of the stretched pulse (red curves) after the BOA and the spectrum of the seed pulse before the BOA (blue curves) for comparison. The (b) RF spectrum and (c) time stretched pulses.

broadband pulse spectrum from the time-stretch source. Figures 5(b) and 5(c) show the spectra of the two orthogonal polarization states from port1 and port2 of the PBS, respectively. The 3-dB bandwidth from port1 and port2 corresponds to 114.9 nm and 130.9 nm, respectively.

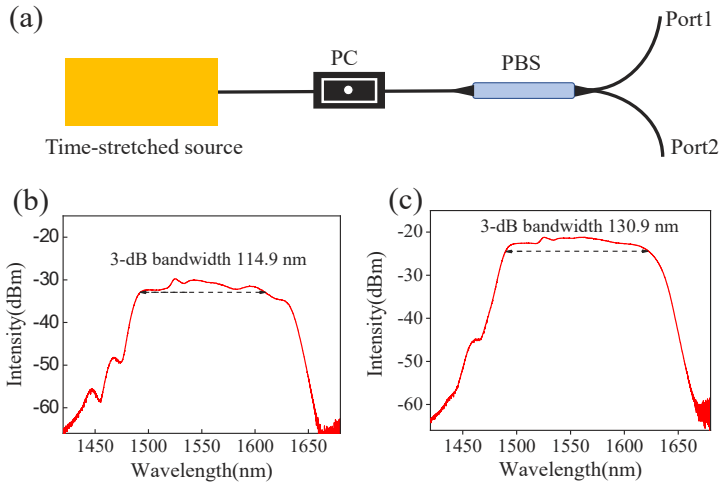

Fig. 5. (a) Experimental setup to measure the spectra of two orthogonal polarizations of the time-stretch source. Spectra after the PBS at one PC state: (b) Spectrum from the port1; (c) Spectrum for the port2.

3.2. Long-term and short-term stability of the swept source

The stability of the swept signal is a key feature for practical applications. In the following, we studied and demonstrated the long-term and short-term stabilities of the swept signal. Figure 6 shows the long-term spectral and output power stability for a duration of six hours at 30-minute time interval. As shown in Fig. 6(a), the profile and intensity of the spectrum remain stable in the 6-hour test period without significant fluctuations. Although the BOA is polarization-dependent and therefore sensitive to the environmental perturbations, we can still obtain a stable swept signal when all the fiber-based components are fixed. Figure 6(b) plots the output power (blue curves) and full-width-at-half-maximum (FWHM) (red curves) of the spectra. From Fig. 6(b), the bandwidth of the flat broadband spectrum remains larger than 136 nm with slight fluctuations of 1.7 nm only. The corresponding output power is ~21 mW with a fluctuation of ~ 4.9 μW, indicating high stability of the output power.

Optics EXPRESS

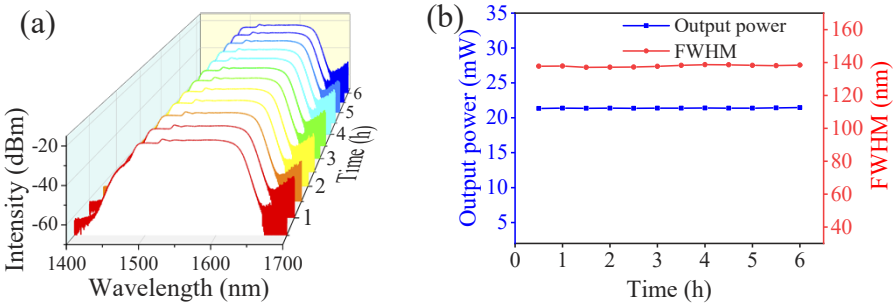

Fig. 6. Long-term stability of the spectra and output power within 6 hours. The (a) spectral stability and (b) 3-dB spectral bandwidth (red curves) and output power (blues curves) of the swept signal.

Apart from the long-term stability of the spectrum and output power, the short-term stability which reflects the coherence and time jitter of the swept signal is also studied. Low coherence of a laser is usually due to strong intensity fluctuations in the time domain, leading to low repeatability of the spectra and temporal pulse forms. A typical example is the spectra of supercontinuum sources. Here, we calculate the degree of similarity between the spectra from different roundtrips to demonstrate the coherence of the laser. The cross correlation of 183,486 roundtrips is used to estimate the spectral similarity [40,41] as shown in Fig. 7(a). To study the influence of the BOA, the spectral similarity via the cross correlation and its histogram before the BOA are shown in Figs. 7(a) and 7(b), respectively, and that after the BOA are shown in Figs. 8(a) and 8(b), respectively. We used the spectrum after the first roundtrip as the reference, while the other spectra are compared to the first one by calculating their cross correlation. From Fig. 7(a), the cross-correlation varies between 0.99875 and 0.99947 over the 183,485 roundtrips, showing a high degree of similarity between the spectra of the time stretched pulse before the BOA. As shown in Fig. 8(a), after the BOA, the cross correlation varies between 0.99962 and 0.99980, indicating a slight improvement in the spectrum similarity. This is because the slight fluctuations of the pulse intensity is eliminated by the BOA working in saturation. The higher intensity pulse will have lower gain while the lower intensity pulse will have higher gain. The insets in Fig. 7(a) and Fig. 8(a) show the variation of the cross-correlations for the first 20 roundtrips. To further study the spectral similarity, histograms of the cross-correlations of the 183,486 consecutive pulse spectra are shown in Fig. 7(b) and Fig. 8(b), before and after the BOA, respectively. The cross-correlation values are distributed near 1, which demonstrates that the spectra have very high degree of similarities. Before the BOA, the ratio of standard deviation to the mean (std/mean) of the cross-correlation was calculated to be only 0.0059%, and that after the BOA is 0.0021%, again as a result of the BOA working in gain saturation.

The short-term stability of the spectral energy is another parameter that needs to be considered for ultrafast imaging. Figures 7(c) and 8(c) show the spectrum energy before and after BOA, respectively. Figure 7(c) depicts the normalized relative spectral energy during 1 ms. Before the BOA, the energy fluctuates between 0.9864 and 1, which is larger than that after the BOA which varies from 0.9913 to 1 as shown in Fig. 8(c). The range of energy fluctuations is only 1% after the BOA indicating that the time stretched pulse has higher short-term stability. We also calculate the histogram of the relative intensity fluctuation with the same 183,486 consecutive spectra. Figure 7(c) shows the histogram before the BOA. The std/mean is 0.17%, indicating that the short-term stability of the from the seed fiber laser spectrum energy is high. The std/mean after the BOA is 0.10%, indicating a lower energy fluctuation because of the gain saturation

Optics EXPRESS

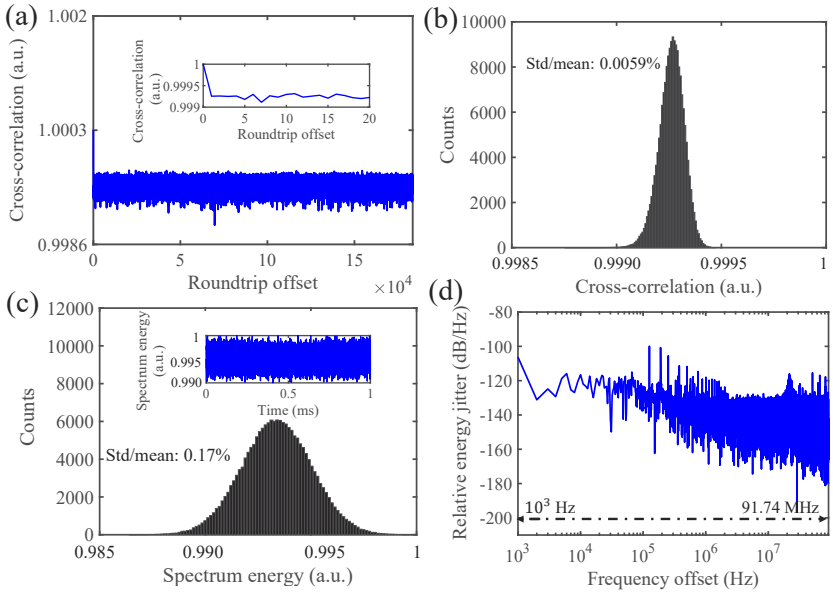

Fig. 7. Short-term stability measurement before the BOA within 1 ms. (a) The cross correlation of 183,486 round trips. The inset shows the cross-correlation of the first 20 round trips. (b) The histogram of the cross correlations in (a). (c) The histogram of the spectral energy and spectrum energy (inset) during 1 ms. (d) The relative energy jitters.

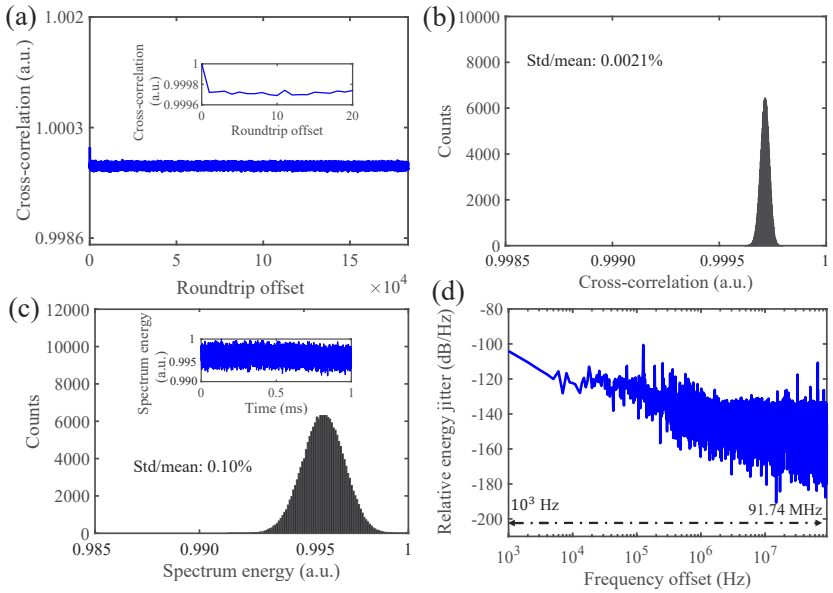

Fig. 8. Short-term stability measurement after the BOA within 1 ms. a) The cross correlation of 183,486 round trips. The inset shows the cross correlation of the first 20 round trips. (b) The histogram of the cross correlations in (a). (c) The histogram of the spectral energy and spectrum energy (inset) during 1 ms. (d) The relative energy jitters.

Optics EXPRESS

effect of the BOA. The low energy jitter shows that the time stretched swept source has high short-term stability, which has high potential for ultrafast imaging and high-speed measurements.

To gain further insight into the relative spectrum energy fluctuation, Figs. 7(d) and 8(d) measure the relative energy jitter [42] before and after the BOA, respectively. The time duration of the pulse train is 1 ms corresponding to 1 kHz frequency resolution. The offset frequency range is ~ 91.74 MHz corresponding to half of the repetition rate of the pulse train. The low-frequency noise are mainly induced by thermal fluctuation in the laser system and the mechanical vibration of the laser cavity caused by the environmental disturbance [42,43]. The average intensity before amplification is about −123.8 dB/Hz in the frequency range from 1 kHz to 1 MHz, which is larger than that of −124.4 dB/Hz after the BOA. At high offset frequency, the noise floor manifests as white noise resulting from the intensity noise of the quantum sources from the fiber laser, photoelectric detector, and other optical elements in the amplification system [42,43]. The noise floor of the relative spectrum energy jitter before the BOA is −135.9 dB/Hz determined from 1 MHz to 91.74 MHz, which is higher than that of −141.7 dB/Hz after the BOA. The low average intensity at low offset frequency and low noise floor at high offset frequency all indicate the small fluctuations of the spectrum energy. The lower intensity noise may be attributed to the design of the seed laser which operates at the near-zero dispersion regime compared with other dispersion regime [20]. Thus, the proposed compact short cavity laser with near-zero dispersion generates a stable output pulse, which serves as the seed laser. By using extra-cavity amplification assisted by the BOA, a stable, flat and broadband time stretched swept source is achieved, which is largely unaffected by the intracavity perturbation and environmental disturbance [42,43] as discussed above.

3.3. SS-OCT system with high axial resolution

The performance of the swept source determines the performance of an SS-OCT system, where the sweep range determines the axial resolution and the sweep rate determines the imaging speed. The proposed time stretched swept source assisted by extra-cavity amplification with the BOA can realize a 183.6 MHz sweep rate and flat broadband sweep range with a 1-dB bandwidth of 93.1 nm and 3-dB bandwidth of 136.7 nm, which will achieve high imaging speed and high axial resolution in an SS-OCT system. Figure 9 shows the point spread function, sensitivity roll-off and the multiple thin glass plates. Figure 9(a) shows the uneven interference fringes acquired in the time domain, which need to be resampled in the frequency domain with the help of the sweep trace. The sweep trace is fitted according to the time to wavelength mapping as shown in Fig. 9(b), which is nonlinear because of third-order and higher order dispersion of the long SMF. Figure 9(c) plots the frequency fluctuation versus wavelength. The swept curve is obtained by a fifteenth-order polynomial fit of the experimental one. The frequency fluctuation is obtained by subtracting fitting one from the experimental one. Figure 9(d) shows that the frequency fluctuation over the swept range of ~ 20 THz is ~16 GHz, which is obtained by a full width at half maximum (FWHM) of the histogram. The number of bins used for the histogram is 1000. The small frequency fluctuation indicates high stability of the swept curve. This highly stable sweep trace is important for precise resampling of the interference signal without the need to repeatedly determine the start point and fit the sweep trace. Figure 9(e) shows the resampled signal. Then by using fast Fourier transform (FFT), the point spread function is shown in Fig. 9(f). The axial resolution by using Gaussian fitting can be as high as 10.8 μm benefitting from the flat broadband spectrum of the swept source, which is higher than that of the SS-OCT systems based on a mode-locked laser [2,4–6,11]. The theoretical axial resolution is given by $\delta z = 2\ln 2 \times \lambda_0^2/(\pi \times \Delta\lambda) \sim 7.82$ μm in the air at the center wavelength of 1559.0 nm, which is higher than the experiment result of 10.8 μm [44]. The discrepancy between the theoretical and experimental result is mainly due to the calibration error in the resampling the experimental data from uniform time to uniform wavelength number which broadens the PSF and lowers the

Optics EXPRESS

axial resolution [2,45]. An asymmetric spectrum profile may also contribute to the lower axial resolution [46–48]. The sensitivity roll-offs of different optical path differences are shown in Fig. 9(g). Sidelobes are observed owing to the non-Gaussian spectrum of the swept source, which can be suppressed by window functions such as Hann, Hamming windows, and adaptive apodization of the spectrum. A flat broadband spectrum can produce a broadband Gaussian envelope by using window functions. The sidelobe suppression ratio can be further enhanced by introducing a complex adaptive sidelobe reduction (CASR) filter, a deviation gating filter (DGF), and the averaging of multiple A-scans, as reported in our previous work [5]. High imaging quality has been demonstrated [5] with reduction of the imaging speed. In this paper, our focus is on high-speed OCT imaging. A sidelobe suppression ratio of 20 dB and extinction ratio of < 40 dB can be used in some highspeed OCT imaging applications [1,2]. The measured sensitivity has no obvious change from 0 to 0.45 mm. When the frequency of the interference pattern reaches the bandwidth limit of the OSC and BPD, the PSF drops dramatically if the optical path difference is further increased [2]. We then apply this high axial resolution OCT system to image the glass plates with a thickness of 0.2 mm. As shown in Fig. 9(h), two pieces of the glass plates corresponding to an imaging depth of 0.4 mm can be distinguished, which matches well with the sensitivity roll-off curve shown in Fig. 9(g). Besides application in OCT imaging, the proposed swept source with high speed and broadband spectrum has other applications such as microscopy [1,2,49,50].

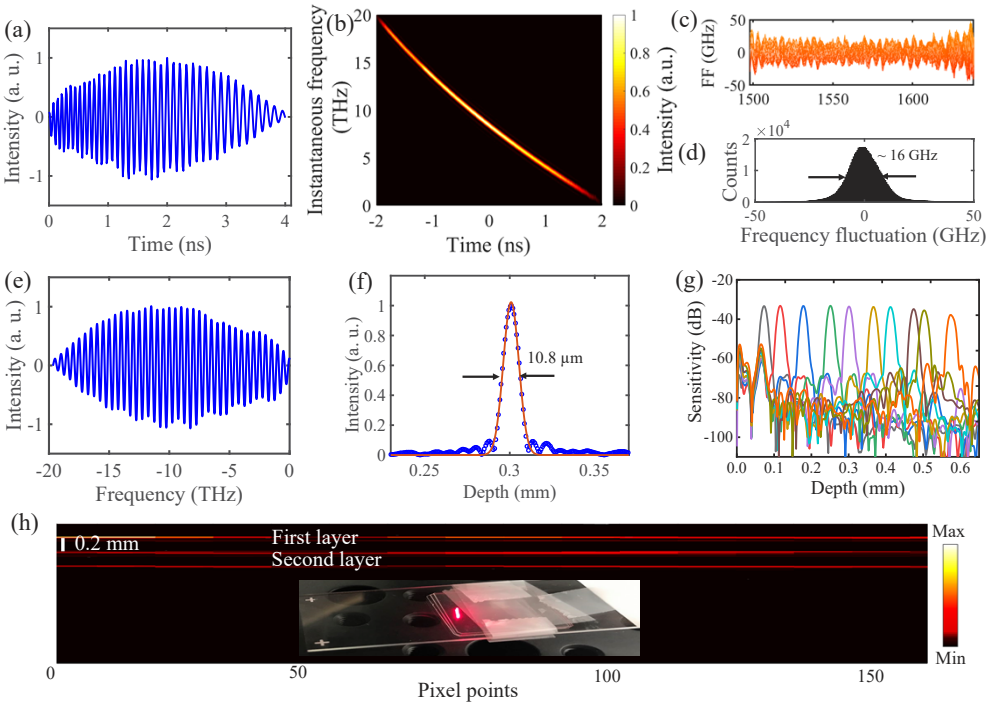

Fig. 9. Performance the SS-OCT system. (a) A single shot interferogram. (b) The swept trace of the laser. (c) The frequency fluctuation of the swept trace, FF: frequency fluctuation. (d) The histogram of the frequency fluctuation. (e) The resampled interference signal. (f) The axial resolution measured in air is 10.8 um. (g) The sensitivity roll-off performance at different depths. (h) The OCT image of two pieces of the glass plates.

Optics EXPRESS

4. Summary

In summary, we have demonstrated a broadband swept source with a flat broadband spectrum, high coherence, and high stability based on extra-cavity amplification. The high coherence of the swept signal is verified by the spectral similarity via calculating the cross correlation. The short-term spectral energy stability is evaluated through the relative energy jitter measurement, which is lower after the BOA benefitting from the gain saturation of the BOA. The high performance swept source with a 1-dB bandwidth of ~93.1 nm and 3-dB bandwidth of 136.7 nm is applied to an OCT system and achieves a high imaging speed of 183.6 MHz and high axial resolution of 10.8 um. The proposed highly stable flat broadband time stretched swept source assisted by extra-cavity amplification and spectral shaping has demonstrated high performance in the SS-OCT system, which has a promising prospect in ultrafast microscopy and 3D LiDAR imaging.

Funding. National Key Research and Development Program of China (2020YFB1805901); National Natural Science Foundation of China (62105274); Science, Technology and Innovation Commission of Shenzhen Municipality (SGDX2019081623060558, JCYJ20210324133406018); Basic and Applied Basic Research Foundation of Guangdong Province (2021A1515012544); Research Grants Council, University Grants Committee of Hong Kong SAR (PolyU152241/18E).

Disclosures. The authors declare no conflicts of interest.

Data availability. Data underlying the results presented in this paper are not publicly available at this time but may be obtained from the authors upon reasonable request.

References

1. X. Wei, A. K. Lau, Y. Xu, K. K. Tsia, and K. K. Wong, "28 MHz swept source at 1.0 mum for ultrafast quantitative phase imaging," Biomed. Opt. Express **6**(10), 3855–3864 (2015).
2. J. Kang, P. Feng, X. Wei, E. Y. Lam, K. K. Tsia, and K. K. Y. Wong, "102-nm, 44.5-MHz inertial-free swept source by mode-locked fiber laser and time stretch technique for optical coherence tomography," Opt. Express **26**(4), 4370–4381 (2018).
3. X. Wei, S. Tan, A. Mussot, A. Kudlinski, K. K. Tsia, and K. K. Wong, "110 nm versatile fiber optical parametric amplifier at 1.0 mum," Opt. Lett. **40**(17), 4090–4093 (2015).
4. H. Chen, Y. Li, D. Huang, F. Li, C. Lu, and P. K. A. Wai, "114 nm broadband all-fiber nonlinear polarization rotation mode locked-laser and time-stretch optical coherence tomography," Opt. Express **29**(21), 33322–33330 (2021).
5. D. Huang, F. Li, Z. He, Z. Cheng, C. Shang, and P. K. A. Wai, "400 MHz ultrafast optical coherence tomography," Opt. Lett. **45**(24), 6675–6678 (2020).
6. X. Wei, J. Xu, Y. Xu, L. Yu, J. Xu, B. Li, A. K. Lau, X. Wang, C. Zhang, K. K. Tsia, and K. K. Wong, "Breathing laser as an inertia-free swept source for high-quality ultrafast optical bioimaging," Opt. Lett. **39**(23), 6593–6596 (2014).
7. D. Huang, Y. Shi, F. Li, and P. K. A. Wai, "Fourier Domain Mode Locked Laser and Its Applications," Sensors **22**(1), 1–5 (2022).
8. R. Huber, M. Wojtkowski, and J. Fujimoto, "Fourier Domain Mode Locking (FDML): A new laser operating regime and applications for optical coherence tomography," Opt. Express **14**(8), 3225–3237 (2006).
9. T. Ideguchi, T. Nakamura, Y. Kobayashi, and K. Goda, "Kerr-lens mode-locked bidirectional dual-comb ring laser for broadband dual-comb spectroscopy," Optica **3**(7), 748 (2016).
10. J. Xu, C. Zhang, J. Xu, K. K. Wong, and K. K. Tsia, "Megahertz all-optical swept-source optical coherence tomography based on broadband amplified optical time-stretch," Opt. Lett. **39**(3), 622–625 (2014).
11. D. Huang, F. Li, C. Shang, Z. Cheng, and P. K. A. Wai, "Reconfigurable time-stretched swept laser source with up to 100 MHz sweep rate, 100 nm bandwidth, and 100 mm OCT imaging range," Photonics Res. **8**(8), 1360 (2020).
12. C. Poudel and C. F. Kaminski, "Supercontinuum radiation in fluorescence microscopy and biomedical imaging applications," J. Opt. Soc. Am. B **36**(2), A139 (2019).
13. Y. Jiang, S. Karpf, and B. Jalali, "Time-stretch LiDAR as a spectrally scanned time-of-flight ranging camera," Nat. Photonics **14**(1), 14–18 (2020).
14. P. Qiao, K. T. Cook, K. Li, and C. J. Chang-Hasnain, "Wavelength-Swept VCSELs," IEEE J. Sel. Top. Quantum Electron. **23**(6), 1–16 (2017).
15. R. Huber, M. Wojtkowski, and J. Fujimoto, "FDLM: A new laser operating regime and applications for optical coherence tomography," in *Cambridge Optics Express* (MIT).
16. K. T. Cook, P. Qiao, J. Qi, L. A. Coldren, and C. J. Chang-Hasnain, "Resonant-antiresonant coupled cavity VCSELs," Opt. Express **27**(3), 1798–1807 (2019).
17. C. D. Lu, M. F. Kraus, B. Potsaid, J. J. Liu, W. Choi, V. Jayaraman, A. E. Cable, J. Hornegger, J. S. Duker, and J. G. Fujimoto, "Handheld ultrahigh speed swept source optical coherence tomography instrument using a MEMS scanning mirror," Biomed Opt Express **5**, 293–311 (2013).

Optics EXPRESS

18. O. O. Ahsen, Y. K. Tao, B. M. Potsaid, Y. Sheikine, J. Jiang, I. Grulkowski, T. H. Tsai, V. Jayaraman, M. F. Kraus, J. L. Connolly, J. Hornegger, A. Cable, and J. G. Fujimoto, "Swept source optical coherence microscopy using a 1310 nm VCSEL light source," Opt. Express **21**(15), 18021–18033 (2013).
19. S. Moon and D. Y. Kim, "Ultra-high-speed optical coherence tomography with a stretched pulse supercontinuum source," Opt. Express **14**(24), 11575–11584 (2006).
20. L. Nugent-Glandorf, T. A. Johnson, Y. Kobayashi, and S. A. Diddams, "Impact of dispersion on amplitude and frequency noise in a Yb-fiber laser comb," Opt. Lett. **36**(9), 1578–1580 (2011).
21. L. Xing, Z. Weiwen, Y. Guang, and C. Jianping, "Direct Generation of 148 nm and 44.6 fs Pulses in an Erbium-Doped Fiber Laser," IEEE Photonics Technol. Lett. **27**(1), 93–96 (2015).
22. X.-D. Wang, M.-Q. Sun, S.-M. Yang, J.-Y. Pan, and S.-W. Li, "Broadband dispersion-managed dissipative soliton and structural soliton molecules in a slight-normal dispersion fiber laser," IEEE Photonics J. **12**, 1–10 (2020).
23. J. Wang, Z. Cai, P. Xu, G. Du, F. Wang, S. Ruan, Z. Sun, and T. Hasan, "Pulse dynamics in carbon nanotube mode-locked fiber lasers near zero cavity dispersion," Opt. Express **23**(8), 9947–9958 (2015).
24. K. Tamura, E. Ippen, H. Haus, and L. Nelson, "77-fs pulse generation from a stretched-pulse mode-locked all-fiber ring laser," Opt. Lett. **18**(13), 1080–1082 (1993).
25. J. Sotor, I. Pasternak, A. Krajewska, W. Strupinski, and G. Sobon, "Sub-90 fs a stretched-pulse mode-locked fiber laser based on a graphene saturable absorber," Opt. Express **23**(21), 27503–27508 (2015).
26. D. Ma, Y. Cai, C. Zhou, W. J. Zong, L. L. Chen, and Z. G. Zhang, "37.4 fs pulse generation in an Er:fiber laser at a 225 MHz repetition rate," Opt. Lett. **35**(17), 2858–2860 (2010).
27. W. Liu, L. Pang, H. Han, W. Tian, H. Chen, M. Lei, P. Yan, and Z. Wei, "70-fs mode-locked erbium-doped fiber laser with topological insulator," Sci. Rep. **6**(1), 19997 (2016).
28. Z. Laszczych and G. Sobon, "Dispersion management of a nonlinear amplifying loop mirror-based erbium-doped fiber laser," Opt. Express **29**(2), 2690–2702 (2021).
29. Y. Lan, Y. J. Song, M. L. Hu, B. W. Liu, L. Chai, and C. Y. Wang, "Enhanced spectral breathing for sub-25 fs pulse generation in a Yb-fiber laser," Opt. Lett. **38**(8), 1292–1294 (2013).
30. F. O. Ilday, F. W. Wise, and T. Sosnowski, "High-energy femtosecond stretched-pulse fiber laser with a nonlinear optical loop mirror," Opt. Lett. **27**(17), 1531–1533 (2002).
31. J. X. Chen, X. Y. Li, T. J. Li, Z. Y. Zhan, M. Liu, C. Li, A. P. Luo, P. Zhou, K. K. Y. Wong, W. C. Xu, and Z. C. Luo, "1.7-mu m dissipative soliton Tm-doped fiber laser," Photonics Res. **9**(5), 873–878 (2021).
32. M. Olivier, V. Boulanger, F. Guilbert-Savary, P. Sidorenko, F. W. Wise, and M. Piche, "Femtosecond fiber Mamyshev oscillator at 1550 nm," Opt. Lett. **44**(4), 851–854 (2019).
33. W. Liu, R. Liao, J. Zhao, J. Cui, Y. Song, C. Wang, and M. Hu, "Femtosecond Mamyshev oscillator with 10-MW-level peak power," Optica **6**(1), 1 (2019).
34. Z. Liu, Z. M. Ziegler, L. G. Wright, and F. W. Wise, "Megawatt peak power from a Mamyshev oscillator," Optica **4**(6), 649–654 (2017).
35. P. Sidorenko, W. Fu, L. G. Wright, M. Olivier, and F. W. Wise, "Self-seeded, multi-megawatt, Mamyshev oscillator," Opt. Lett. **43**(11), 2672–2675 (2018).
36. C. Ma, A. Khanolkar, Y. Zang, and A. Chong, "Ultrabroadband, few-cycle pulses directly from a Mamyshev fiber oscillator," Photonics Res. **8**(1), 65 (2019).
37. P. Sidorenko and F. Wise, "Generation of 1 microJ and 40 fs pulses from a large mode area gain-managed nonlinear amplifier," Opt. Lett. **45**(14), 4084–4087 (2020).
38. P. Sidorenko, W. Fu, and F. Wise, "Nonlinear ultrafast fiber amplifiers beyond the gain-narrowing limit," Optica **6**(10), 1328–1333 (2019).
39. M. J. Connelly, *Semiconductor optical amplifiers* (Springer Science & Business Media, 2007).
40. I. S. Kudelin, S. Sugavanam, M. Chernysheva, A. C. Peacock, N. G. R. Broderick, and J. M. Dudley, "Correlation of solitons in bidirectional mode-locked fibre laser," in *Nonlinear Optics and its Applications* 2020, (2020).
41. B. Li, S. W. Huang, Y. Li, C. W. Wong, and K. K. Y. Wong, "Panoramic-reconstruction temporal imaging for seamless measurements of slowly-evolved femtosecond pulse dynamics," Nat. Commun. **8**(1), 61 (2017).
42. J. Kim and Y. Song, "Ultralow-noise mode-locked fiber lasers and frequency combs: principles, status, and applications," Adv. Opt. Photonics **8**(1), 1 (2016).
43. R. Paschotta, A. Schlatter, S. C. Zeller, H. R. Telle, and U. Keller, "Optical phase noise and carrier-envelope offset noise of mode-locked lasers," Appl. Phys. B **82**(2), 265–273 (2006).
44. J. A. Izatt and M. A. Choma, "Theory of Optical Coherence Tomography," Opt. Coherence Tomography **1**, 47–72 (2008).
45. E. Azimi, B. Liu, and M. E. Brezinski, "Real-time and high-performance calibration method for high-speed swept-source optical coherence tomography," J. Biomed. Opt. **15**(1), 016005 (2010).
46. R. Tripathi, N. Nassif, J. S. Nelson, B. H. Park, and J. F. de Boer, "Spectral shaping for non-Gaussian source spectra in optical coherence tomography," Opt. Lett. **27**(6), 406–408 (2002).
47. R. Huber, M. Wojtkowski, K. Taira, J. G. Fujimoto, and K. Hsu, "Amplified, frequency swept lasers for frequency domain reflectometry and OCT imaging: design and scaling principles," Opt. Express **13**(9), 3513–3528 (2005).
48. A. C. Akcay, J. P. Rolland, and J. M. Eichenholz, "Spectral shaping to improve the point spread function in optical coherence tomography," Opt. Lett. **28**(20), 1921–1923 (2003).

Optics EXPRESS

49. W. Xiaoming, A. K. S. Lau, T. T. W. Wong, Z. Chi, K. K. M. Tsia, and K. K. Y. Wong, "Coherent Laser Source for High Frame-Rate Optical Time-Stretch Microscopy at 1.0 μm," IEEE J. Sel. Top. Quantum Electron. **20**(5), 384–389 (2014).
50. S. Hu, J. Yao, M. Liu, A. P. Luo, Z. C. Luo, and W. C. Xu, "Gain-guided soliton fiber laser with high-quality rectangle spectrum for ultrafast time-stretch microscopy," Opt. Express **24**(10), 10786–10796 (2016).